

---

This is an electronic reprint of the original article.  
This reprint may differ from the original in pagination and typographic detail.

Michieletto, Daniele; Alberti, Luigi; Belahcen, Anouar

## Optimization of Printed Synchronous Reluctance Rotor Based on Bézier Curves

*Published in:*

2024 International Conference on Electrical Machines, ICEM 2024

*DOI:*

[10.1109/ICEM60801.2024.10700207](https://doi.org/10.1109/ICEM60801.2024.10700207)

Published: 01/01/2024

*Document Version*

Peer-reviewed accepted author manuscript, also known as Final accepted manuscript or Post-print

*Please cite the original version:*

Michieletto, D., Alberti, L., & Belahcen, A. (2024). Optimization of Printed Synchronous Reluctance Rotor Based on Bézier Curves. In *2024 International Conference on Electrical Machines, ICEM 2024 (Proceedings (International Conference on Electrical Machines))*. IEEE. <https://doi.org/10.1109/ICEM60801.2024.10700207>

---

This material is protected by copyright and other intellectual property rights, and duplication or sale of all or part of any of the repository collections is not permitted, except that material may be duplicated by you for your research use or educational purposes in electronic or print form. You must obtain permission for any other use. Electronic or print copies may not be offered, whether for sale or otherwise to anyone who is not an authorised user.

# Optimization of Printed Synchronous Reluctance Rotor Based on Bézier Curves


1<sup>st</sup> Daniele Michieletto

dept. of Industrial Engineering  
University of Padova  
Padova, Italy

daniele.michieletto@phd.unipd.it 


2<sup>nd</sup> Luigi Alberti

dept. of Industrial Engineering  
University of Padova  
Padova, Italy

luigi.alberti@unipd.it 

3<sup>rd</sup> Anouar Belahcen

dept. of Electrical Engineering and Automation  
Aalto University  
Espoo, Finland

anouar.belahcen@aalto.fi 

**Abstract**—This paper deals with the optimization of a multi-barrier synchronous reluctance rotor, in which the flux barriers are parameterized using Bézier curves. With this type of modeling, it is possible to explore more complex geometries that can be realized with new additive manufacturing techniques. A two-step optimization based on the NSGA-II genetic algorithm is proposed in the paper. In the first part, barriers are optimized using a simplified analytical model. In the second part, the rotor geometry is optimized using finite element analysis. Finally, a more detailed investigation is performed to calculate the overall performance of the optimized solution and compare them with those of a previously manufactured prototype.

**Index Terms**—Synchronous reluctance motor, electrical machines, additive manufacturing, optimization, fluid barriers, Bézier curves, laser powder bed fusion, L-PBF

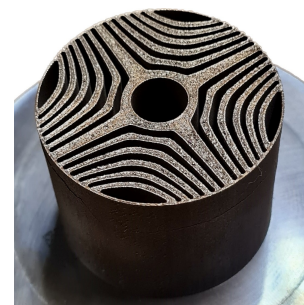
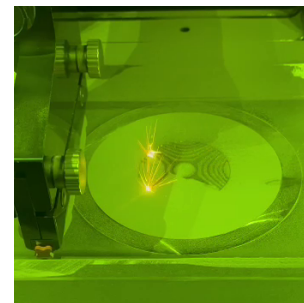
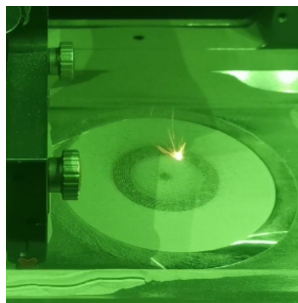
## I. INTRODUCTION

The optimization and improvement of components or products play a key role in any sector, both technically and commercially. In recent years, electrification has demanded increasingly high-performing and efficient electric motors capable of meeting several requirements of various economic and industrial sectors. In this scenario, Additive Manufacturing (AM) [1], [2] emerges as an interesting technology for producing components ready for use and high performance, specifically designed to be manufactured using these new production techniques. In particular, AM allows for:

- greater design flexibility by enabling the creation of intricate geometries and structures that may include undercuts or empty spaces,
- optimizing material utilization, minimizing waste almost entirely,
- enhancing the strength-to-weight ratio of the final product.

As for the electric motors are concerned, several examples are reported in literature about the adoption of AM in windings, mechanical structures, thermal exchangers and permanent magnets fabrication [3]–[6]. Less attention has been given to the manufacture of ferromagnetic components, such as the rotors of Synchronous Reluctance (SynRel)

This project has been funded in the frame of BIRD 2023 call of the Padova University, project id ALBE BIRD23 01 entitled "Design and realization of a PM assisted synchronous reluctance machine with additive manufacturing technology".



(a) Ferromagnetic core [12]

(b) SynRel rotor [10], [11]

Fig. 1: Fabrication of ferromagnetic components by L-PBF. The laser light spot can be seen in the top pictures.

motors. These components prove to be good candidates to be produced by AM techniques thanks to the absence of permanent magnets. An example of a Switched Reluctance motor fabricate using AM can be found in [7], while some investigations of the properties of the printed material are presented in [8], [9]. In [10], [11] the design and realization of a SynRel motor by means of AM has been presented. In [12] the electromagnetic characterization of the printed material has been investigated in order to obtain the actual BH curve of Silicon-Iron printed structures.

This paper introduces an optimization process for complex rotor topologies designed to be fabricated by AM techniques. First, the optimal number of flux barriers is investigated, given the main sizes of the electric motor and winding. Next, the design of the rotor structures based on the fluid shaped flux barriers [13]–[15] is considered. Then, a design based on the

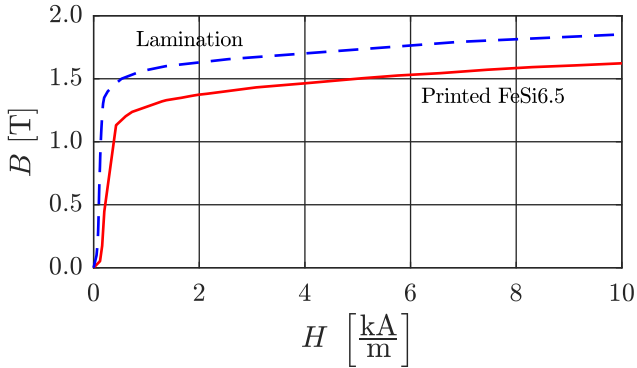


Fig. 2: BH curve of commercial lamination [16] and printed ferromagnetic material.

TABLE I: Motor main parameters

No. of slots	$Q$	24	–
No. pole pairs	$p$	2	–
Airgap	$g$	0.3	mm
Outer diameter	$D_e$	80	mm
Inner diameter	$D_i$	45	mm
Shaft diameter	$D_{sh}$	12	mm
Axial length	$L_{stk}$	30	mm
Slot cross-section area	$S_{slot}$	47	mm <sup>2</sup>

description of the flux barrier geometry using Bézier curves is proposed. Lastly, the overall performance of the optimized rotor structure are computed to quantify the improvements achieved compared to the first realized prototype [10], [11].

## II. MANUFACTURING PROCESS

This section briefly presents the additive manufacturing process and the samples manufactured with this technology.

### A. Laser Powder Bed Fusion

The AM technique called Laser Powder Bed Fusion (L-PBF) consists of melting metal powder, in this specific case ferromagnetic powder (FeSi6.5), to produce the desired geometry. The ferromagnetic powder is spread in thin layers over the building platform where a laser fuses specific regions to create the desired structure. This process is repeated until the component is completely fabricated.

Fig. 1 shows the realization of a ferromagnetic core and a SynRel rotor. The ferromagnetic core (Fig. 1a) was manufactured to measure the electromagnetic characteristics of the printed material. Fig. 2 shows the comparison between BH curve of a commercial lamination [16] and that of the printed material. It can be seen that for field intensity values above 2 kA/m the two curves are quite close. Therefore, the printed material has good electromagnetic properties and can be a good candidate for the fabrication of ferromagnetic components that operate at high flux density, such as the rotor of SynRel machines. More detailed information about the electromagnetic characterization can be found in [12].

The rotor prototype (Fig. 1b) was manufactured to demonstrate the possibility of realizing SynRel rotors using

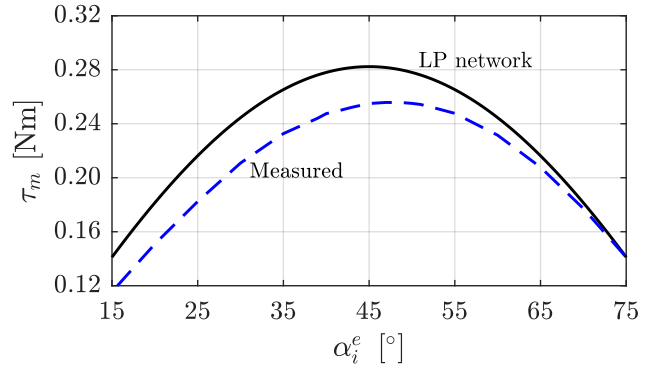


Fig. 3: Torque versus current angle. Comparison between LP magnetic network and experimental tests on the prototype of Fig. 1b.

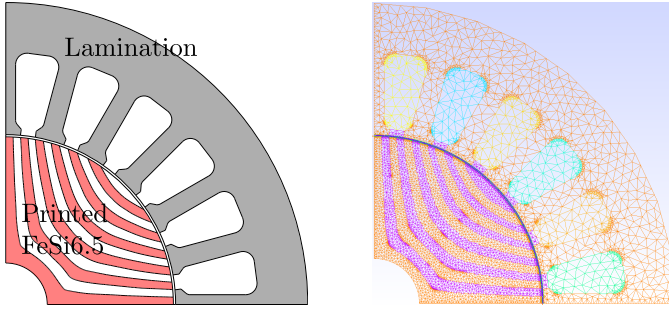
AM techniques. The rotor geometry was designed with state of art methodology with fluid shaped flux barriers. Table I reports the main parameters of the motor.

### B. Lumped parameters magnetic network

The integration of additive manufacturing (AM) methods into electrical machine fabrication introduces new opportunities for achieving complex rotor shapes, necessitating a reevaluation of current modeling approaches. The possibility of creating rotor structures with numerous flux barriers requires a model that facilitates the analysis and design of these solutions. For this reason a lumped parameters (LP) magnetic network [17] was adopted to quick analyze multi-barrier SynRel rotors. The model was tested comparing its results with the experimental measurements carried out on the SynRel prototype of Fig. 1b. Fig. 3 shows the comparison of the torque versus current angle  $\alpha_i^e$ . There is good agreement between the values obtained with the magnetic network and the experimental results. Slight differences were expected since saturation effects were not considered. This model can be used as a first approach in the preliminary design of the rotor structure, particularly to derive the optimal number of barriers once the main characteristics of the motor (size, winding, number of poles, etc.) have been selected.

### C. Finite element model

Finite element analyses were used to more accurately calculate the performance of the prototype, considering the non-linearity of the magnetic material and the effects of saturation. The finite element model was developed considering the two different magnetic properties (see Fig. 2) for the stator and rotor as shown in Fig. 4a. The measured BH curve of the printed material is an essential information necessary to know to predict precisely the performance of the motor. The AM prototype was tested and the experimental results were compared with the simulation data. Table II summarize the performance of the motor for the nominal current (6 A) and an overload at twice the nominal current



(a) Geometry and ferromagnetic materials

(b) Mesh

Fig. 4: Finite element model

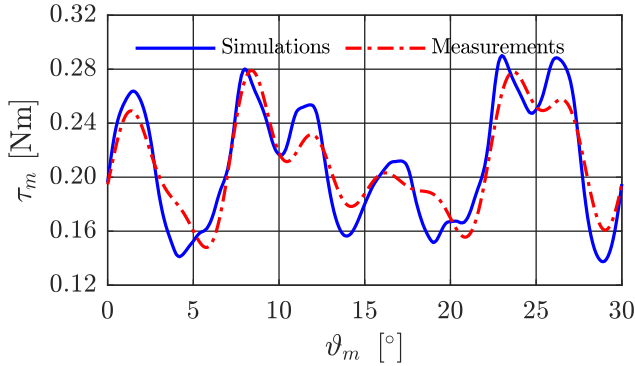


Fig. 5: Torque versus rotor position. Comparison between simulation and experimental tests at nominal current.

(12 A) where  $\tau_m$  is the average torque of the motor,  $\Delta\tau_m$  is the torque ripple,  $\alpha_i^e$  is the electrical angle of the current space vector and  $\delta_T$  is the torque per volume unit which was computed as:

$$\delta_T = \frac{4T}{1000\pi D_e^2 L_{stk}} \quad (1)$$

Fig 5 shows the comparison between simulations and experimental tests where the torque versus rotor position is considered at the nominal current.

### III. OPTIMIZATION ALGORITHM AND DESIGN PROCEDURE

Several optimization algorithms were studied and developed in literature [18]. In this work a genetic algorithm called NSGA-II has been adopted [19], [20].

The proposed design procedure can be summarized in three main steps:

- preliminary design to determine the optimal number of flux barriers;
- first optimization of a fluid shaped barrier rotor;
- second optimization based on Bézier description of the flux barriers.

These steps will be described in detail in the following subsections.

TABLE II: Motor performance.

SynRel motor proposed in [10], [11]					
Simulation results					
$I$ [A]	$\tau_m$ [N m]	$\Delta\tau_m$ [%]	$\alpha_i^e$ [°]	MTPA	$\delta_T$ [Nm/L]
6	0.21	72.71	45		1.39
12	0.80	62.39	49		5.24
Experimental measurements					
$I$ [A]	$\tau_m$ [N m]	$\Delta\tau_m$ [%]	$\alpha_i^e$ [°]	MTPA	$\delta_T$ [Nm/L]
6	0.21	65.43	45		1.39
12	0.80	59.37	49		5.24

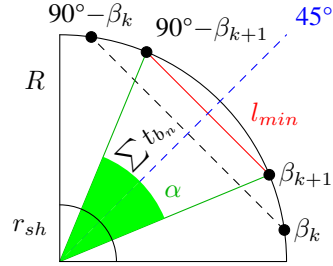


Fig. 6: Constraint sketch of the magnetic network.

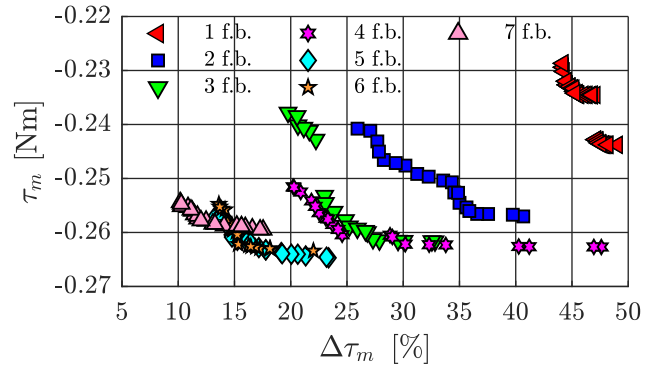


Fig. 7: Comparison of pareto fronts of rotors with different number of flux barriers. Results obtained with LP network.

#### A. Optimal number of flux barriers

Preliminary design to derive the optimal number of barriers is performed to simplify the optimization process, since the total number of variables to be optimized depends on the number of flux barriers. The lumped parameters magnetic network introduced in Sec. II-B was used to accomplish this task with the aim of achieving a good compromise between model accuracy and computational time.

Given the motor main parameters and the number of barriers, the magnetic network depends on the length  $l_n$ , thickness  $t_b$  and  $\beta$  angles that characterize each flux barrier. However, each of these quantities must satisfy specific constraints to avoid considering unfeasible solutions (overlapping barriers). Eq. 2 summarizes all these constraints where  $k_{ir}$  is a coefficient which considers that a minimum thickness of iron is required between barriers,  $R$  is the rotor diameter and  $r_{sh}$  is the shaft diameter. Fig. 6 shows a sketch

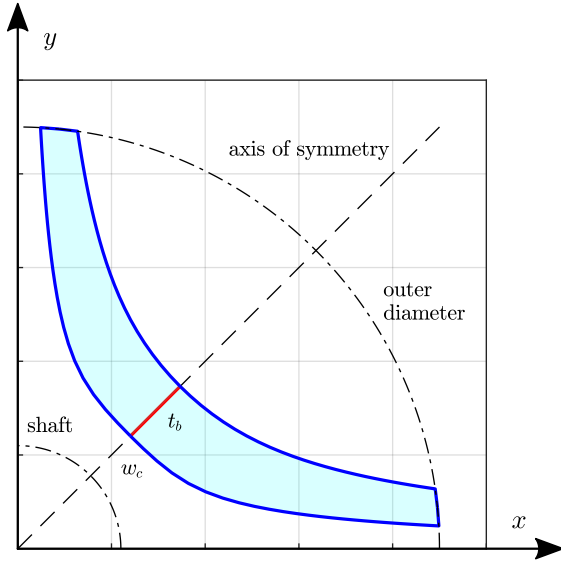


Fig. 8: Example of fluid shaped flux barrier.

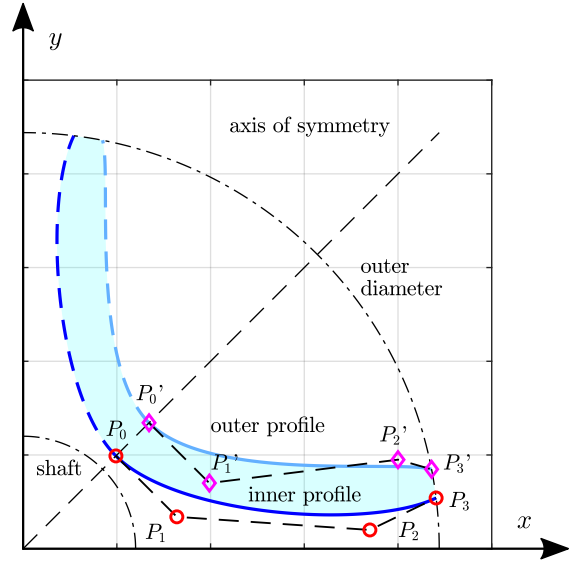


Fig. 10: Example of Bézier based flux barrier.

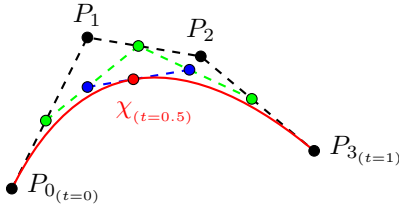


Fig. 9: Example of Bézier cubic curve.

of the constraints to be observed.

$$\begin{cases} \beta_k < \beta_{k+1} < 45^\circ \\ l_{min} < l_n < l_{n+1} \\ \sum t_{b_n} < R - r_{sh} - k_{ir} \end{cases} \quad l_{min} = 2R \sin(\alpha) \quad (2)$$

The optimization process was carried out for different numbers of barriers, starting with the simplest case, a single-barrier rotor, and successively increasing the number by one unit until no appreciable improvements in motor performance were achieved. Fig. 7 shows the comparison of the different pareto fronts obtained with this approach, where the average torque versus the torque ripple of the motors is reported. Each front is related to a specific number of flux barriers. It can be seen that increasing the number of barriers results in improved performance of the electric motor. However, considering more than five barriers does not result in significant performance enhancement, so such solutions would add complexity to the rotor without having any real return in terms of performance. Therefore, five flux barriers has been chosen as the optimal configuration for the following steps.

### B. Fluid shaped barriers optimization

A first optimization based on fluid shaped barriers was developed in order to obtain rotor topologies with good performance by exploiting a well-known design methodology. The nominal working point of the motor ( $I = 6$  A) was selected to be optimized, trying to maximize the average torque and minimize the torque ripple. The rotor topology can be obtained choosing the thickness  $t_b$  of flux barriers and the iron thickness  $w_c$  and solving the fluid equations [15]. In this way, the coordinates of the points which describe the fluid profiles can be computed and the finite element model of the rotor can thus be realized and solved. Fig. 8 shows an example of a rotor with two pole pairs where a fluid shaped barrier is drawn. To avoid unfeasible geometries the constraint  $\sum_{j=1}^{n_{bar}} t_{b_j} + \sum_{j=1}^{n_{bar}+1} w_{c_j} = R - r_{sh}$  needs to be satisfied.

### C. Bézier based flux barrier optimization

A Bézier curve [21] is a particular parametric curve which is described by a set of control points. It has been adopted because it allows to describe effectively the shape of the flux barriers with a limited number of points. The proposed approach considers cubic (4 control points) Bézier curves described by the equation (3), to model the profile of the flux barrier, where  $\chi$  stands for the Bézier curve profile,  $P_0$ ,  $P_1$ ,  $P_2$  and  $P_3$  are the control points of the curve and  $t$  is the parameter that belongs to  $[0, 1]$  which allows to compute each point of  $\chi$ .

$$\chi = (1-t)^3 P_0 + 3t(1-t)^2 P_1 + 3t^2(1-t) P_2 + t^3 P_3 \quad (3)$$

$$0 \leq t \leq 1$$

Fig. 9 shows an example of cubic Bézier curve with its control points. By joining multiple Bézier curves together, it is possible to create the profile of a flux barrier as shown in

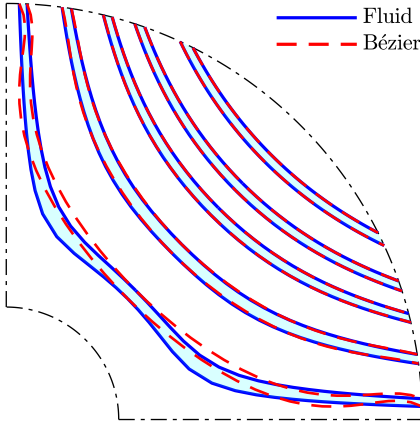


Fig. 11: Example of Bézier profiles computed from fluid shaped flux barriers.

TABLE III: Control point definition of the Bézier based barrier profile.

Coordinates			Boundaries		
	$x$	$y$		lower	upper
$P_0$	$r \cos(\pi/4)$	$r \sin(\pi/4)$	$r$	$r_{sh}$	$R$
$P_1$	$P_{1x}$	$P_{1y}$	$P_{2x}$	0	$R$
$P_2$	$P_{2x}$	$P_{2y}$	$P_{1y}, P_{2y}$	0	$R \sin(\pi/4)$
$P_3$	$R \cos(\vartheta_3)$	$R \sin(\vartheta_3)$	$\vartheta_3$	$0^\circ$	$45^\circ$

Fig. 10 where, for the sake of simplicity, a single barrier of a rotor with two pole pairs is shown and the symmetry of the poles is also exploited to further simplify the description of the barrier. More specifically, each flux barrier is defined by a couple of Bézier curve (inner and outer profile) and each curve is describe by 4 control points that can be computed as reported in Tab. III where variables to be optimized are highlighted in bold type. The following assumptions were considered:

- the point  $P_0$  belongs to the axis of symmetry,
- the point  $P_3$  belongs to the rotor circumference,
- the tangent of the profile at point  $P_0$  must be perpendicular to the axis of symmetry.

Some constraints need to be satisfied to avoid intersections between Bézier curves that would lead to unfeasible geometries. Eq. (4) summarizes all these conditions.

$$\begin{cases} r(k) < r(k+1) \\ P_{1x}(k) < P_{2x}(k) \\ P_{1y}(k) < P_{1y}(k+1) \\ P_{2y}(k) < P_{2y}(k+1) \\ P_{1x}(k)^2 + P_{1y}(k)^2 > r_{sh}^2 \\ P_{2x}(k)^2 + P_{2y}(k)^2 < R^2 \\ \vartheta_3(k) < \vartheta_3(k+1) \end{cases} \quad k \in \{1, \dots, 2n_{bar} - 1\} \quad (4)$$

To simplify the search for sets of control points describing feasible rotor topologies, the optimized profiles of fluid barriers were used to calculate the respective Bézier curves.

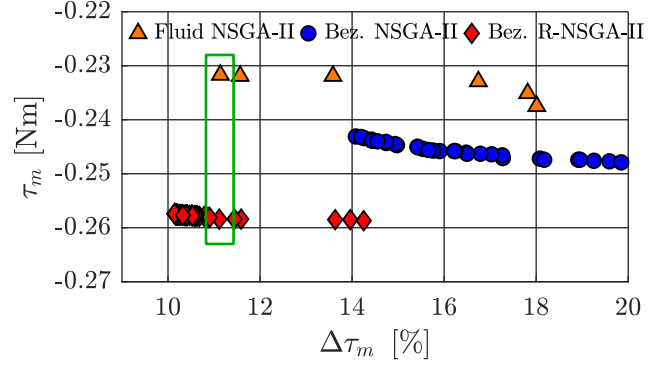


Fig. 12: Pareto comparison. Results obtained with finite element analysis.

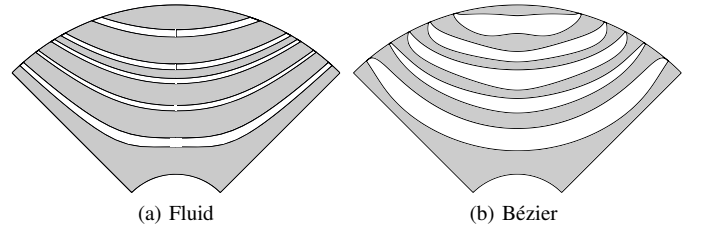


Fig. 13: Example of optimized rotor solutions. Green rectangle of Fig. 12

Fig. 11 shows an example of a fluid barrier rotor structure on which the respective Bézier curves calculated with a fitting function were superimposed. The set of solutions obtained with this method was used as the initial solution of the Bézier-based optimization process.

#### D. Optimization results

All the optimization procedures were characterized by a population of 120 samples and a time stop criterion set to 24 hours. Fig. 12 shows the comparison of the pareto fronts obtained from the two optimizations presented in III-B and III-C. It can be noticed that the rotor structures modeled with Bézier curves result in better performance especially in terms of average torque. To try to further improve the average torque and torque ripple, a modified version of NSGA-II called R-NSGA-II [22] was tested. The difference between the two algorithms is that in R-NSGA-II, target values are set for  $\tau_m$  and  $\Delta\tau_m$  that the algorithm tries to satisfy as a priority. Therefore, the optimization process will tend to favor the reproduction of intermediate pareto front solutions close to these target values. As a result, the optimization process is improved and the pareto front is found more quickly.

An example of optimized rotor structures is shown in Fig. 13. In particular, these geometries refer to the solutions contained in the green rectangle of Fig 12. These topologies were chosen since they have the same torque ripple. It can be observed that the Bézier curves allow for more freedom in the flux barrier profile, which is thicker in the inner zones, but

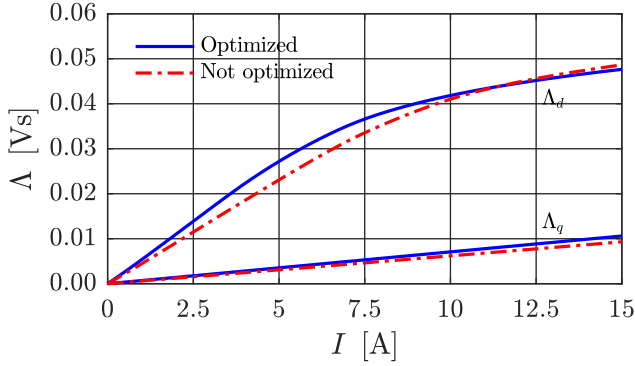


Fig. 14: Direct and quadrature flux-linkage. Comparison between optimized and not optimized topology. Simulation results.

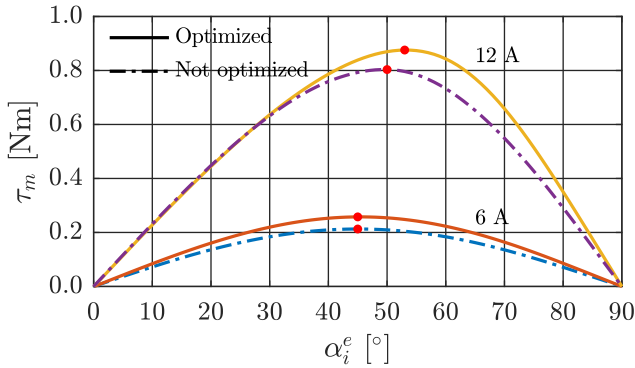
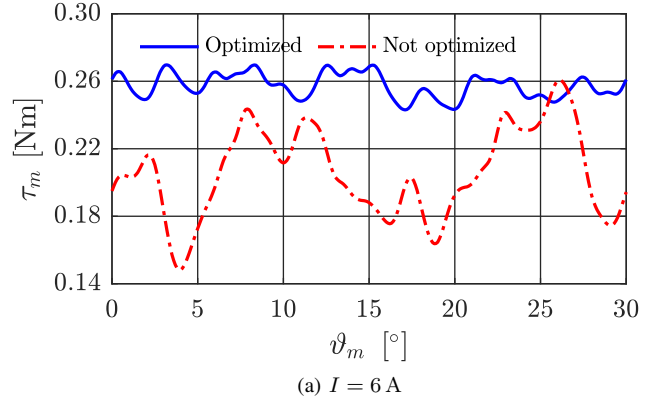


Fig. 15: Torque versus current angle for  $I_n$  and  $2I_n$ . Comparison between optimized and not optimized rotor topology. Red dots highlight the MTPA working points. Simulation results.

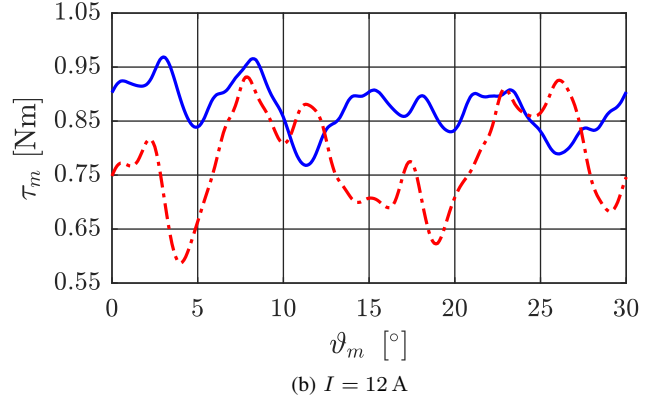
still tends to narrow by increasing the iron portion relative to the airgap portion.

#### IV. OPTIMIZED MOTOR PERFORMANCE

In this section, the performance of the optimized motor (Fig. 13b referred to as optimized) will be discussed in detail. Specific finite element simulations were conducted to estimate different quantities that characterize the electrical machine. The results are compared with the simulations of the motor shown in Fig. 1b (referred to as not optimized) to exhibit the improvements achieved with the proposed optimization. The comparison of the flux-linkages of the two rotor geometries is shown in Fig. 14 where the increasing on the  $d$ -axis flux-linkage in the optimized geometry can be observed particularly at nominal current. Fig. 15 shows the torque versus current angle  $\alpha_i^e$  while Fig. 16 exhibits the torque ripple of the motor for the nominal current and an overload at twice the rated current. In both cases  $\alpha_i^e$  was set equal to the MTPA angle respective to the considered current. Table IV shows the numerical values. It can be observed that the proposed solution significantly improves the performance of the electric machine.



(a)  $I = 6$  A



(b)  $I = 12$  A

Fig. 16: Torque versus rotor position for  $I_n$  and  $2I_n$ . The current angles  $\alpha_i^e$  is the equal to the MTPA angles. Comparison between optimized and not optimized rotor topology. Simulation results.

TABLE IV: Motor performance comparison.

SynRel motor proposed in [10], [11]					
$I$ [A]	$\tau_m$ [N m]	$\Delta\tau_m$ [%]	$\alpha_i^e$ [°] MTPA	$\delta_T$ [Nm/L]	
6	0.21	53.82	45	1.39	
12	0.80	44.78	49	5.24	
Optimized SynRel motor					
$I$ [A]	$\tau_m$ [N m]	$\Delta\tau_m$ [%]	$\alpha_i^e$ [°] MTPA	$\delta_T$ [Nm/L]	
6	0.26	10.36	45	1.72	
12	0.87	22.97	53	5.77	

Considering the rated current, the average torque is increased by 23.8% with a torque ripple reduction of 43.5%. The same is true if an overload of  $2I_n$  is considered. In this case, the average torque is improved by 8.75%, while the torque ripple is reduced by 21.8%.

#### V. CONCLUSION

In this paper, a design procedure to realize SynRel rotors using AM was studied. The topology of the barrier was described using Bézier curves. In this way, the flux barriers can be defined with a limited number of control points while still maintaining a wide freedom in the profile. This type of modeling was used together with the NSGA-II genetic algorithm to optimize the rotor geometry and

improve the average torque and torque ripple at the nominal operating point. The proposed procedure achieves significant improvements in motor performance.

#### BIOGRAPHY SECTION

**Daniele Michieletto** received his Bachelor of Science in Energy Engineering and Master of Science in Electrical Engineering degrees from the University of Padova, Padova, Italy, in 2018 and 2020, respectively. He is now pursuing a Doctor of Philosophy in Industrial Engineering at the University of Padova. His research interests focus on the design of electrical machines, with an emphasis on additive manufacturing production processes.

**Luigi Alberti** (SM'20) received the Laurea and the Ph.D. degrees in electrical engineering from the University of Padova, Padova, Italy, in 2005 and 2009, respectively. From 2009 to 2012, he was a Research Associate at the University of Padova. In 2012, he moved to the Faculty of Science and Technology, Free University of Bozen-Bolzano, Italy, to start research and educational activities in the field of electrical engineering and electrical machines. He is currently an Associate Professor with the Department of Industrial Engineering, University of Padova, working on design, analysis, and control of electric machines and drives, with particular interest in renewable energies and more electric vehicles.

**Anouar Belahcen** (Senior Member, IEEE) was born in Morocco in 1963. He received the M.Sc. (Tech.) and Ph.D. (Tech.) degrees from Aalto University (former Helsinki University of Technology), Espoo, Finland, in 1998 and 2004, respectively. He is currently a Professor of power and energy with Aalto University, where he has been the Vice Dean of education with the School of Electrical Engineering since 2020. His research interests are numerical modeling of electrical machines, characterization and modeling of magnetic materials, coupled magneto-mechanical problems, magnetic forces, magnetostriction, and fault diagnostics of electrical machines.

#### REFERENCES

- [1] K. V. Wong and A. Hernandez, "A review of additive manufacturing," *ISRN Mechanical Engineering*, vol. 2012, pp. 1–10.
- [2] G. N. Mhetre, V. S. Jadhav, S. P. Deshmukh, and C. M. Thakar, "A review on additive manufacturing technology," *ECS Transactions*, vol. 107, no. 1, pp. 15 355–15 374.
- [3] N. Simpson, D. J. North, S. M. Collins, and P. H. Mellor, "Additive manufacturing of shaped profile windings for minimal AC loss in electrical machines," *IEEE Transactions on Industry Applications*, vol. 56, no. 3, pp. 2510–2519.
- [4] B. G. Compton, J. W. Kemp, T. V. Novikov, R. C. Pack, C. I. Nlebedim, C. E. Duty, O. Rios, and M. P. Paranthaman, "Direct-write 3D printing of NdFeB bonded magnets," *Materials and Manufacturing Processes*, vol. 33, no. 1, pp. 109–113.
- [5] R. Wrobel and B. Mecrow, "A comprehensive review of additive manufacturing in construction of electrical machines," *IEEE Transactions on Energy Conversion*, vol. 35, no. 2, pp. 1054–1064.
- [6] A. Selema, M. N. Ibrahim, and P. Sergeant, "Additively manufactured ultralight shaped-profile windings for hf electrical machines and weight-sensitive applications," *IEEE Transactions on Transportation Electrification*, vol. 8, no. 4, pp. 4313–4324, 2022.
- [7] L. Gargalis, V. Madonna, P. Giangrande, R. Rocca, M. Hardy, I. Ashcroft, M. Galea, and R. Hague, "Additive manufacturing and testing of a soft magnetic rotor for a switched reluctance motor," *IEEE Access*, vol. 8, pp. 206 982–206 991, 2020.
- [8] H. Tiismus, A. Kallaste, A. Belahcen, T. Vaimann, A. Rassõlkin, and D. Lukichev, "Hysteresis measurements and numerical losses segregation of additively manufactured silicon steel for 3d printing electrical machines," *Applied Sciences*, vol. 10, no. 18, 2020. [Online]. Available: <https://www.mdpi.com/2076-3417/10/18/6515>
- [9] H. Tiismus, A. Kallaste, A. Belahcen, M. Tarraste, T. Vaimann, A. Rassõlkin, B. Asad, and P. Shams Ghahfarokhi, "Ac magnetic loss reduction of slm processed fe-si for additive manufacturing of electrical machines," *Energies*, vol. 14, no. 5, 2021. [Online]. Available: <https://www.mdpi.com/1996-1073/14/5/1241>
- [10] D. Michieletto and L. Alberti, "Design and realization of a synchronous reluctance motor with printed rotor," in *IECON 2022 – 48th Annual Conference of the IEEE Industrial Electronics Society*. IEEE.
- [11] —, "On the performance of PMAREL and REL synchronous motor prototypes with printed rotor," in *2023 IEEE Energy Conversion Congress and Exposition (ECCE)*, pp. 3953–3958.
- [12] D. Michieletto, L. Alberti, F. Zanini, and S. Carmignato, "Electromagnetic characterization of silicon-iron additively manufactured cores for electric machines," *Energies*, vol. 17, no. 3, 2024. [Online]. Available: <https://www.mdpi.com/1996-1073/17/3/650>
- [13] R. M. Reza, "Synchronous reluctance machine in variable speed drives applications," Ph.D. dissertation, KTH Royal Institute, Stockholm, Sweden, 2011.
- [14] G. Bacco and N. Bianchi, "Design criteria of flux-barriers in synchronous reluctance machines," *IEEE Transactions on Industry Applications*, vol. 55, no. 3, pp. 2490–2498, 2019.
- [15] A. Credo, G. Fabri, L. D. Leonardo, and M. Villani, "Synchronous reluctance motor with fluid shaped barriers: preliminary and optimized design procedures," in *IECON 2021 – 47th Annual Conference of the IEEE Industrial Electronics Society*, 2021, pp. 1–6.
- [16] Voestalpine, "Isovac 350-50a datasheet," Available online: [https://www.voestalpine.com/division\\_stahl/content/download/32782/347314/file/DB\\_isovac\\_350-50A\\_E\\_280715.pdf](https://www.voestalpine.com/division_stahl/content/download/32782/347314/file/DB_isovac_350-50A_E_280715.pdf), 01/2018 Last Updated, accessed: 09 January 2024.
- [17] D. Michieletto and L. Alberti, "A scalable analytical model for printed multi-barrier reluctance rotor," in *2023 IEEE International Electric Machines & Drives Conference (IEMDC)*. IEEE.
- [18] G. Venter, *Review of Optimization Techniques*. John Wiley & Sons, Ltd, 2010. [Online]. Available: <https://onlinelibrary.wiley.com/doi/abs/10.1002/9780470686652.eac495>
- [19] K. Deb, A. Pratap, S. Agarwal, and T. Meyarivan, "A fast and elitist multiobjective genetic algorithm: NSGA-II," *IEEE Transactions on Evolutionary Computation*, vol. 6, no. 2, pp. 182–197, 2002.
- [20] K. Deb, K. Sindhya, and T. Okabe, "Self-adaptive simulated binary crossover for real-parameter optimization," in *Proc. 9th Annu. Conf. Genetic and Evol. Comput. (GECCO)*, New York, NY, USA, 2007, p. 1187–1194.
- [21] E. Rafajłowicz, "Fast algorithm for generating bernstein-bézier polynomials," *Journal of Computational and Applied Mathematics*, vol. 51, no. 3, pp. 279–292, 1994. [Online]. Available: <https://www.sciencedirect.com/science/article/pii/037704279200110U>
- [22] K. Deb and J. Sundar, "Reference point based multi-objective optimization using evolutionary algorithms," in *Proc. 8th Annu. Conf. Genetic and Evol. Comput. (GECCO)*, New York, NY, USA, 2006, p. 635–642.